

Integrated control of an air-breathing hypersonic vehicle considering the safety of propulsion system

Chengkun Lv^{1a}, Juntao Chang^{*1} and Lei Dai^{2b}

¹Harbin Institute of Technology, Harbin, 150001, PR China

²Shenyang Airplane Design and Research Institution, Shenyang, 110013, PR China

(Received October 9, 2021, Revised December 3, 2022, Accepted December 16, 2022)

Abstract. This paper investigates the integrated control of an air-breathing hypersonic vehicle considering the safety of propulsion system under acceleration. First, the vehicle/engine coupling model that contains a control-oriented vehicle model and a quasi-one-dimensional dual-mode scramjet model is established. Next, the coupling process of the integrated control system is introduced in detail. Based on the coupling model, the integrated control framework is studied and an integrated control system including acceleration command generator, vehicle attitude control loop and engine multivariable control loop is discussed. Then, the effectiveness and superiority of the integrated control system are verified through the comparison of normal case and limiting case of an air-breathing hypersonic scramjet coupling model. Finally, the main results show that under normal acceleration case and limiting acceleration case, the integrated control system can track the altitude and speed of the vehicle extremely well and adjust the angle deflection of elevator to offset the thrust moment to maintain the attitude stability of the vehicle, while assigning the two-stage fuel equivalent ratio to meet the thrust performance and safety margin of the engine. Meanwhile, the high-acceleration requirement of the air-breathing hypersonic vehicle makes the propulsion system operating closer to the extreme dangerous conditions. The above contents demonstrate that considering the propulsion system safety will make integrated control system more real and meaningful.

Keywords: air-breathing hypersonic vehicle; attitude controller; integrated control; multivariable controller; scramjet safety

1. Introduction

Air-breathing hypersonic vehicles have been proposed as an ideal way to launch reliable and affordable two-stage-to-orbit (TSTO) transportation into low earth orbit (Burcham *et al.* 1998, Rodriguez *et al.* 2008, Yao *et al.* 2010, Lee *et al.* 2015). The development of air-breathing hypersonic vehicles faces great challenges in hypersonic aerodynamics, high-performance power propulsion, and integrated flight and propulsion control system design. The integrated control of airframe and propulsion system is one of the keys to achieve hypersonic flight of air-breathing vehicles. There are complicated interactions between the engine dynamics and vehicle characteristics, which brings challenges to the integrated control system design of air-breathing

*Corresponding author, Professor, E-mail: changjuntao@hit.edu.cn

^aPh.D. Student, E-mail: lvchengkun@hit.edu.cn

^bPh.D., E-mail: dailei@sia.cn

hypersonic vehicles (Bolender and Doman 2005, Bolender 2009, Zheng *et al.* 2019). As a matter of fact, air-breathing engines may be trapped in danger because of the direct influence of flight conditions. Changes in the attitude of the aircraft can affect the flow field in the inlet tract, resulting in abnormal engine operating conditions. After the second flight test of the X-51A failed due to inlet unstart, the safety characteristics of the engine gradually came to the attention of researchers. In acceleration, the high thrust requirement of the engine makes the inlet near operating boundary and unstart problem of the inlet has plagued the design of hypersonic aircrafts (Li *et al.* 2019). Therefore, ensuring the safety of propulsion system is a significant content of the integrated control for an air-breathing hypersonic vehicle.

In recent years, guidance and control methods for air-breathing hypersonic vehicles have emerged. Groves *et al.* (2006) discussed two linear quadratic optimal control methods, setpoint tracking control and regulator control, for the air-breathing hypersonic vehicle. At the same time, considering the saturation characteristic of the control input, the anti-windup control for statically unstable system was proposed. Sigthorsson *et al.* (2008) developed a hypersonic vehicle model with additional canard, designed output feedback controller with internal model control (IMC) method, and studied linear parameter varying (LPV) control. Fiorentini *et al.* (2009) adopted a robust semi-global gain assignment method and adaptive control to design sub-controllers and formed a closed loop global controller. With the rapid development of nonlinear control, many nonlinear control methods had been applied to air-breathing hypersonic vehicles to ensure velocity and altitude tracking performance or anti-interference ability (Mooij 2001, Huo *et al.* 2006, Wang *et al.* 2019, An *et al.* 2020). Meanwhile, various advanced intelligent methods, including fuzzy theory and reinforcement learning, were combined with nonlinear control to solve velocity and altitude tracking control of air-breathing hypersonic vehicles because the strong nonlinear approximation capabilities (Mu *et al.* 2016, Cheng *et al.* 2019). For integrated flight and propulsion control, Zhang *et al.* (2016) systematically investigated integrated flight/propulsion modeling and optimal control of the distributed propulsion configuration with boundary layer inhalation and hypercyclic characteristics. Li *et al.* (2021) designed a controller based on pole assignment, where the control parameters can be adjusted according to real-time aerodynamic data to solve the integrated control problem of flight-propulsion coupling. Yu *et al.* (2022) proposed a GA-LQR-based controller design method for a TBCC-powered air-breathing hypersonic vehicle and validated it with aircraft climb and mode transition conditions.

From the above, the control of the air-breathing hypersonic vehicle mainly focuses on the velocity and altitude of the aircraft, while ignoring the safety problem of engine. The multivariable control considering safety of the engine is rare. In the existing research, the engine often uses the fitting result under different input variables to couple an integrated model, and the thrust in the fitting model is affected by the fuel and flight conditions. Obviously, the safety of scramjet is not taken seriously and can hardly be guaranteed in such a coupling model. Therefore, we propose an integrated control scheme that couples the longitudinal rigid body dynamics model of the air-breathing hypersonic vehicle and a quasi-one-dimensional dual-mode scramjet model. Under the acceleration command, the vehicle attitude controller and engine multivariable controller are used to complete the integrated control of the acceleration.

The main innovation of this paper is to solve the acceleration control problem of the air-breathing hypersonic vehicle with dual-mode scramjet by the integrated control system. This method ensures the tracking performance of the air-breathing hypersonic vehicle and the safety of the engine. Meanwhile, the verification of the acceleration control process shows that the dual-mode scramjet is easy to run close to the inlet safety boundary when confronts with the

requirement of high acceleration. Thus, it is necessary to consider the safety problem of scramjet in the integrated control. This paper is organized as follow. Section 2 introduces the control-oriented integrated coupling model. The whole integrated control system is design in Section 3. The verification under different acceleration commands is carried out in Section 4. Section 5 summarizes the paper.

2. Problem formulation

The control research is carried out based on the integrated airframe–propulsion model established in the reference (Lv *et al.* 2020). The control-oriented model of an air-breathing hypersonic vehicle used in this paper is discussed by Parker *et al.* (2007). Based on the analytical model of air-breathing hypersonic vehicles proposed in Bolender and Doman (2005) and Bolender and Doman (2007), Parker further fitted the force and torque into polynomial forms, and then obtained the mathematical model for control system design. In addition, the control-oriented model of vehicles ignores the elastic mode in this research. Thus, the longitudinal rigid body dynamics model of air-breathing hypersonic vehicles is described as

$$\begin{cases} \dot{V} = \frac{F \cdot \cos \alpha - D}{m} - g \cdot \sin(\theta - \alpha) \\ \dot{\alpha} = -\frac{1}{m \cdot V} \cdot (L + F \cdot \sin \alpha) + q + \frac{g}{V} \cdot \cos(\theta - \alpha) \\ \dot{H} = V \cdot \sin(\theta - \alpha) \\ \dot{\theta} = q \\ \dot{q} = \frac{M}{I_{yy}} \end{cases} \quad (1)$$

Where V is velocity, α is angle of attack, H is altitude, θ is pitch angle, q is pitch rate, F is thrust, D is drag, L is lift, M is pitching moment, m is vehicle mass, I_{yy} is moment of inertia, g is acceleration of gravity.

The L and D of aircraft are related to the attitude and inflow condition, and the pitching moment M is usually divided into aerodynamic one and thrust one. L , D and M can be calculated by the following polynomial fitting formula

$$\begin{cases} L = \frac{1}{2} \rho V^2 s C_L(\alpha, \delta_e) \\ D = \frac{1}{2} \rho V^2 s C_D(\alpha, \delta_e) \\ M = z_T F + \frac{1}{2} \rho V^2 s \bar{c} C_M(\alpha, \delta_e) \end{cases} \quad (2)$$

Where ρ is density, s is reference area, δ_e is angle deflection of elevator, z is the force-arm of the propulsion system, \bar{c} is reference length of engine. In addition, $C_L(\alpha, \delta_e)$, $C_D(\alpha, \delta_e)$ and $C_M(\alpha, \delta_e)$ are polynomial fitting functions of lift L , drag D and pitching moment M respectively, see Appendix A.

In this research, the propulsion system of air-breathing hypersonic vehicles is a quasi-one-dimensional dual-mode scramjet (Ma *et al.* 2018, Ma *et al.* 2019), which is constructed using quasi-one-dimensional Euler equation. Unlike the zero-dimensional model used by previous

researchers, the one-dimensional model can reflect the physical processes inside the engine and the distributed parameter characteristics in the engine flow field (Cui 2014, Lee 2015), and can obtain the real engine performance parameters and safety margin, which can be used to accurately analyze the coupling characteristics between the aircraft and the engine. The main function of the model is to calculate the thrust and inlet steady margin by simplifying the shock wave in the inlet and integrating the pressure in the combustion. The one-dimensional model can be expressed as follows

$$\begin{cases} F = f_1(H, Ma, \alpha, \phi_1, \phi_2) \\ \xi = f_2(H, Ma, \alpha, \phi_1, \phi_2) \end{cases} \quad (3)$$

Where ξ is inlet steady margin, Ma is Mach number, ϕ_1 is first stage fuel equivalent ratio, ϕ_2 is second stage fuel equivalent ratio, f_1 and f_2 are nonlinear differentiable functions.

Although the control-oriented model of the air-breathing hypersonic vehicle given in Eq. (1) studies the influence of thrust on the vehicle, it lacks judgment on the safety of engine. Unfortunately, the issue of inlet unstart has puzzled the hypersonic propulsion system for decades. To avoid this problem, we consider the inlet steady margin in the integrated coupling model. The vehicle/engine coupling model contains a longitudinal rigid body dynamics model of the air-breathing hypersonic vehicle and a quasi-one-dimensional dual-mode scramjet model. The block diagram of integrated coupling model for the air-breathing hypersonic vehicle is shown in Fig. 1. As a matter of fact, there are strong effects between aircraft and engine. First, the scramjet model simulates thrust by present flight conditions (α , Ma and H) and fuel equivalent ratios (ϕ_1 and ϕ_2). Then, the aircraft model reaches a new equilibrium point under the influence of the thrust. Therefore, the attitude of the vehicle also affects the incoming flow conditions of the engine. Finally, the engine will reach a new state containing thrust and safety performance outputs.

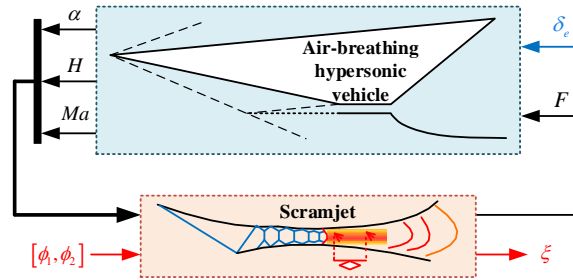


Fig. 1 The integrated coupling process of the air-breathing hypersonic vehicle

The air-breathing hypersonic vehicle model in Eq. (1) is a statically unstable system which is hard to self-stabilize. This makes it difficult to analyze the dynamic characteristic of the vehicle and the coupling effect between the vehicle and engine. Thus, a stable control system of the vehicle is significant. Many linear control methods have been quite reliable after a long period of development. To adopt linear control technique, we must linearize the aircraft and engine models in certain trim point.

Near a certain trimming point, the linearization result of the air-breathing hypersonic vehicle model can be express as

$$\begin{cases} \dot{x}_v = A_v x_v + B_v u_v \\ y_v = C_v x_v \end{cases} \quad (4)$$

Where $x_v = [V, \alpha, H, \theta, q]^T$, $u_v = [\delta_e, F]^T$, $y_v = H$.

One-dimensional dual-mode scramjets involve a large amount of aerothermodynamic knowledge, which makes it difficult to design control system. Similarly, the linear model of the engine at a certain fixed point can be described as

$$\begin{cases} \dot{x}_p = A_p x_p + B_p u_p \\ y_p = C_p x_p \end{cases} \quad (5)$$

Where x_p is internal implicit state variable of scramjet, $u_p = [\varphi_1, \varphi_2]^T$, $F_p = [F, \zeta]^T$.

3. Integrated control system design

3.1 Framework of integrated control

Integrated control system of air-breathing hypersonic vehicle is essentially a multi-loop control system with internal and external loops. Firstly, since the vehicle is a statically unstable system, it is necessary to obtain closed-loop stability by designing an attitude controller of the vehicle. We present the aircraft controller based on LQR method to ensure the attitude stability of the aircraft. In fact, under certain engine thrust, the controller adjusts angle deflection of elevator δ_e to keep attitude stable, and we can get corresponding flight parameters such as velocity, angle of attack, track angle, altitude, and Mach number. In this way, the dual-mode scramjet is also affected by the incoming flow conditions from the attitude of the aircraft. There are great coupling effects between aircraft and engine. In addition to providing thrust, the engine control system also considers safety requirements. The vehicle/engine integrated control system is mainly composed of the outer loop system with acceleration command generator, and the inner loop system with vehicle attitude controller and engine multivariable controller. Fig. 2 shows the block diagram of the integrated control system.

The outer loop of integrated control system adopts the acceleration command generator, which provides acceleration command signals to control the integrated system and complete the specified

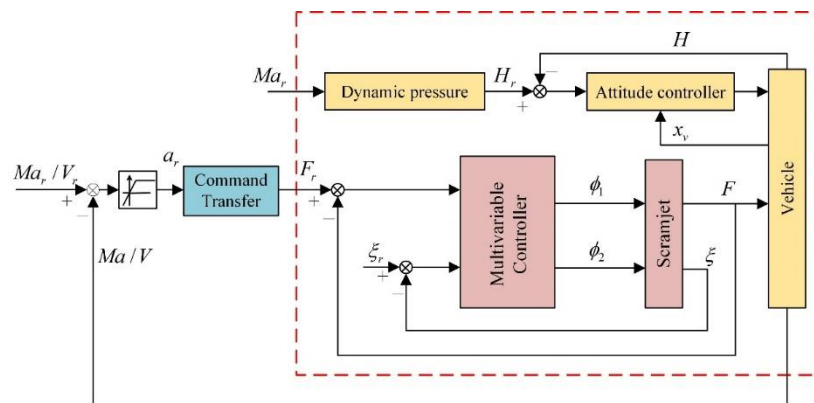


Fig. 2 Block diagram of the air-breathing hypersonic vehicle integrated control system

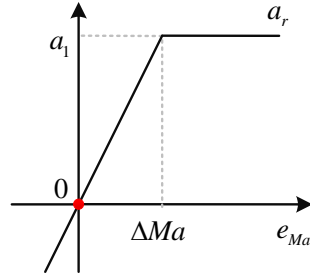


Fig. 3 The piecewise linear structure of Mach number tracking error converted into acceleration command

operation process. The conversion process of acceleration command a_r and thrust command $F_r = a_r m + D$, where D is drag and m is vehicle mass. After we convert the acceleration command to the thrust command and make a difference with the feedback thrust from engine output, the thrust tracking error is used as the input of the engine controller. Combined with safety needs, the engine controller adjusts the two-stage fuel equivalent ratio to achieve multivariable control and obtain the thrust output of the scramjet. Meanwhile, the vehicle attitude controller ensures the flight attitude stability by adjusting the angle deflection of elevator δ_e under current engine output thrust. Eventually, the vehicle operates according to the constant dynamic pressure condition to reach the specified Ma target value and complete the flight mission.

3.2 Acceleration command generator

In general, flight commands are altitude and velocity in much research of aircraft control. However, the engine system is responsible for the acceleration in fact. The velocity or flight Mach number that the aircraft system feeds back to the engine system usually can hardly be selected as the control command, but needs to be further converted into acceleration, which is then converted into appropriate thrust control command through thrust-drag balance.

According to the mission requirements of acceleration and cruise, the flight speed command is set as the Mach number. The Mach number tracking error of the closed-loop control system is

$$e_{Ma} = Ma_r - Ma \quad (6)$$

The Mach number tracking error is converted into acceleration command. Because the command cruise Ma does not contain acceleration information, the piecewise linear structure is used to generate acceleration command. In Fig. 3, we present the generation process of the acceleration command.

First, assume cruise Ma is 5.5 and acceleration demand value a_1 is 0.15 g. The piecewise linear structure is divided into two parts, one is the horizontal part, which corresponds to the uniform acceleration command, and the other is the slanted part, which corresponds to the acceleration command in the transitional section and the cruising section. Among them, the setting parameter ΔMa is the trigger point for the acceleration command to smoothly enter the transition section. Then, the formula for calculating the acceleration is shown below

$$a_r = \begin{cases} a_1 & , e_{Ma} > \Delta Ma \\ \frac{a_1}{\Delta Ma} e_{Ma} & , e_{Ma} \leq \Delta Ma \end{cases} \quad (7)$$

Table 1 Trim point of the air-breath hypersonic vehicle linear model

Trim point parameters	Value	Unit
Ma	4.5	—
α	0.2	deg
H	20681	m
θ	0.2	deg
q	0	deg/s

Comparing the size of e_{Ma} and ΔMa , there will be two cases. If $e_{Ma} > \Delta Ma$, we determine that the aircraft needed to set acceleration command $a_r = a_1$. The value of a_1 can be set artificially, like 0.15g. However, the acceleration of is limited by the ultimate performance of the scramjet. If $e_M < \Delta Ma$, the vehicle is recognized to enter the cruise from the transition, and the acceleration command a_r will become zero as the Ma reach to Ma_r . Finally, combined with thrust-drag balance, the thrust command F_r of engine can be calculated by acceleration command a_r .

3.3 Vehicle attitude control loop

There are 5 state variables $x_v = [V, \alpha, H, \theta, q]^T$ and 2 output variables $u_v = [\delta_e, F]^T$ in a hypersonic vehicle model. The linear model is given in Eq. (4). To meet the requirements of attitude stability and altitude tracking, we add the integral of aircraft altitude tracking error as a state variable

$$\begin{aligned} \omega &= \int (r_H - H) dt = \int (r_H - C_v x_v) dt, \\ C_v &= [0 \ 0 \ 1 \ 0 \ 0] \end{aligned} \quad (8)$$

In this work, it is assumed that the rigid body dynamic system of the aircraft can be fully state feedback (Baumann *et al.* 2013). The trim point is $x_{v,0} = [V_0, \alpha_0, H_0, \theta_0, q_0]^T$ and $u_v = \delta_{e,0}$. We chose to fly at constant dynamic pressure and the value of the trim point is given in Table 1.

The new state variable of the aircraft is the deviation between the aircraft state and the trim point. The new control variable of the aircraft is the deviation between the control variable of the aircraft and the trim point. The state equation of the linearized system is expressed in an incremental form as follows

$$\begin{cases} \hat{x}_v = x_v - x_{v,0} \\ \hat{u}_v = u_v - u_{v,0} \end{cases} \quad (9)$$

After variable substitution, the aircraft stability and height tracking control problem are transformed into a typical linear quadratic optimal state controller design problem. The form of the augmented system is shown as follows

$$\begin{aligned} \dot{\hat{x}}_{v,a} &= A_{v,a} \hat{x}_{v,a} + B_{v,a} \hat{u}_{v,a} + B_{v,r} r_H \\ \begin{bmatrix} \dot{\hat{x}}_v \\ \dot{\omega} \end{bmatrix} &= \begin{bmatrix} A_v & 0 \\ -C_v & 0 \end{bmatrix} \begin{bmatrix} \hat{x}_v \\ \omega \end{bmatrix} + \begin{bmatrix} B_v \\ 0 \end{bmatrix} \hat{u}_v + \begin{bmatrix} 0 \\ I \end{bmatrix} r_H \end{aligned} \quad (10)$$

The above control objectives are expressed as quadratic performance indicators

$$J(\hat{x}_{v,a}, \hat{u}_v) = \frac{1}{2} \int_0^\infty [\hat{x}'_{v,a}(t) Q \hat{x}_{v,a}(t) + \hat{u}'_v(t) Q \hat{u}_v(t)] dt \quad (11)$$

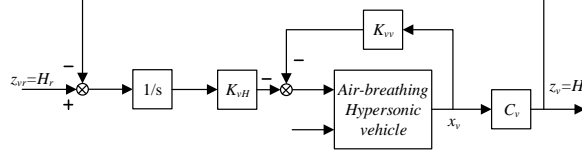


Fig. 4 Aircraft stabilization/tracking controller structure

Table 2 Fixed point of the dual-mode scramjet linear model.

Fixed point parameters	Value	Unit
Ma	5	—
α	0	deg
H	22000	m
φ_1	0.265	—
φ_2	0.275	—

Where $Q=Q'=diag([1\ 1\ 1\ 1\ 1\ 1])>0$, $R=R'=10>0$.

The control law can be expressed in the following form Huo *et al.* (2006)

$$\hat{u}_v = -(R^{-1}B'_{v,a}N)\hat{x}_{v,a} = -K_v\hat{x}_{v,a} \quad (12)$$

We can get N by solving the algebraic Riccati equation

$$Q + NA_{v,a} + A'_{v,a}N - NB_{v,a}R^{-1}B'_{v,a}N = 0 \quad (13)$$

Where $N=N'>0$.

The complete structure of the aircraft controller can be obtained as follows

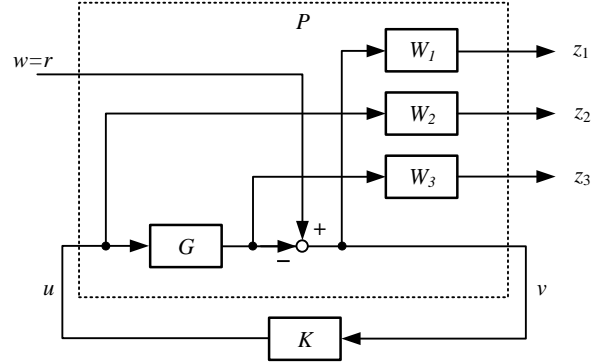
$$u_v = u_{v,0} - K_v\hat{x}_{v,a} = u_{v,0} - K_{vv}(x_v - x_{v,0}) - K_{vH} \int (z_{vr} - C_v x_v) dt \quad (14)$$

The controller structure is often referred to as a linear quadratic proportional integral filter structure (Kuipers *et al.* 2007). K_{vv} is used to control attitude stability, which ensures that the pitching rate of the aircraft is controlled near zero. K_{vH} is used to control altitude tracking, which realizes the flight of the aircraft along the trajectory of the specified altitude. The aircraft control loop is shown in Fig. 4.

3.4 Engine multivariable control loop

In this section, the weighted H_∞ mixed sensitivity problem (Echols *et al.* 2013) is used to design the multivariable controller of the scramjet. According to the engine model shown in Eq. (5), the input of the scramjet engine are two-stage fuel equivalent ratios, and the output are thrust and inlet steady margin. The fixed point of the dual-mode scramjet linear model is shown in Table 2.

In general, the method requires converting the controlled plant into a standard form. The block diagram of H_∞ standard problem considering instruction tracking is shown in Fig. 4, and the closed-loop control system can be described as


 Fig. 5 The block diagram of H_∞ standard problem considering instruction tracking

$$\begin{bmatrix} z \\ v \end{bmatrix} = P(s) \begin{bmatrix} w \\ u \end{bmatrix} = \begin{bmatrix} P_{11}(s) & P_{12}(s) \\ P_{21}(s) & P_{22}(s) \end{bmatrix} \begin{bmatrix} w \\ u \end{bmatrix} \quad (15)$$

$$u = K(s) v \quad (16)$$

Where $G(s)$ is the controlled plant, $P(s)$ is the generalized controlled plant, $K(s)$ is the controller, w is the external input signal, u is the controller output signal, z is the performance output signal, and v is the controller input signal.

In Fig. 5, there are three weight functions, namely performance weight function W_1 , input weight function W_2 and output weight function W_3 . In general, H_∞ synthesis needs to examine the transfer function from the external input w to the performance output z . The transfer function from w to z can be expressed by a linear fractional transformation

$$z = F_l(P, K)w \quad (17)$$

From Fig. 5, it is not difficult to know

$$F_l(P, K) = \begin{bmatrix} W_1 S \\ W_2 K S \\ W_3 T \end{bmatrix} \quad (18)$$

Among them, $S = (I + GK)^{-1}$ is the sensitivity function, and $T = GK(I + K)^{-1}$ is the complementary sensitivity function that known as the closed-loop transfer function of the system. Obviously, $I = T + S$.

Weighted H_∞ Mixed Sensitivity Problem (Doyle *et al.* 1989). Referring to the general control structure shown in Fig. 5, the weighted H_∞ mixed sensitivity problem is to find a real-rational proper internally stabilizing controller K that satisfies

$$\|F_l(P, K)\|_\infty = \max_{\omega} \bar{\sigma}(F_l(P, K)(j\omega)) < \gamma \quad (19)$$

Where $\|\cdot\|_\infty$ is the H_∞ norm, which means the peak of the maximum singular value $\bar{\sigma}$ of $F_l(P, K)(j\omega)$. The stabilizing controller K can be solved by Gahinet and Apkarian (1994).

In the controller design, the weighting functions W_1 , W_2 and W_3 , which are shown in Fig. 5, will be exploited as design parameters. In this research, we choose the weighting functions as

$$\begin{cases} W_1 = \text{diag}\left(\frac{0.5s+0.8}{s+0.004}, \frac{0.5s+0.8}{s+0.004}\right) \\ W_2 = \text{diag}(0.8, 0.6) \\ W_3 = \text{diag}(1, 1) \end{cases} \quad (20)$$

4. Main result

In this section, we will verify the effectiveness and superiority of the proposed integrated control considering the attitude stability of vehicle and the safety of propulsion system through simulation experiments of the nonlinear vehicle/engine coupling model. The dynamic climbing control process of the integrated control system is given under the normal case of $a_r=0.15$ g. Then, the similar flight objective is carried out under the limiting case of $a_r=0.25$ g to illustrate the impact of propulsion system safety on the integrated coupling system. We only pay attention to the acceleration of the system to Ma 5.5. Thus, all simulations describe dynamic responses of vehicle and engine from Ma 5.0 to Ma 5.5.

4.1 Normal case ($a_r=0.15$ g)

The simulation of the air-breathing hypersonic vehicle is presented to verify the effectiveness and superiority of the integrated control system at first. We make the air-breathing hypersonic vehicle operate from Ma 5.0 to Ma 5.5 with an acceleration of 0.15 g under the command of the integrated control system. By observing the output of the aircraft and engine system before reaching Ma 5.5, the coupling control results of the integrated control system considering the safety of the propulsion system are studied. The scramjet must be work in a high-performance state in acceleration. We set the inlet steady margin command signal as 0.3 due to the analysis of the engine performance. However, the difference is that the thrust command is obtained by ensuring the overall thrust-drag balance under the joint action of the acceleration command generator and the vehicle attitude control loop. Obviously, the thrust command changes dynamically throughout the flight to meet the needs of the aircraft. In Fig. 6, the solid blue line and the dotted red line show the state output of the aircraft attitude control loop when the air-breathing hypersonic vehicle climbs at an acceleration of 0.15 g. With the similar acceleration command, Fig. 7 indicates the performance output of the engine multivariable control loop by solid blue line and the dotted red line, and Fig. 8 gives the controller output of both control loops by solid blue line and dotted blue line.

It can be seen from Fig. 6(a) that the entire climb process starts at 25 seconds and reaches the expected flying Ma 5.5 at about 131 seconds. At the beginning of acceleration, the flight angle of attack suddenly decreased from the previous steady-state value of 0.78° to around 1.1° in Fig. 6(b). With the intervention of the aircraft attitude control system, the angle of attack stabilized at around 0.68° at 40 seconds, which means that the attitude control loop has successfully completed the role of stabilizing the vehicle during the acceleration. Fig. 6 (c) and (e) show that the climbing altitude is rising continuously, and the altitude error drops from 54 meters to 50 meters. The altitude tracking error of the aircraft is decreasing during acceleration, which indicates that the controller considering the altitude error integral plays an effective role. Fig. 6 (d) and (f) show that the

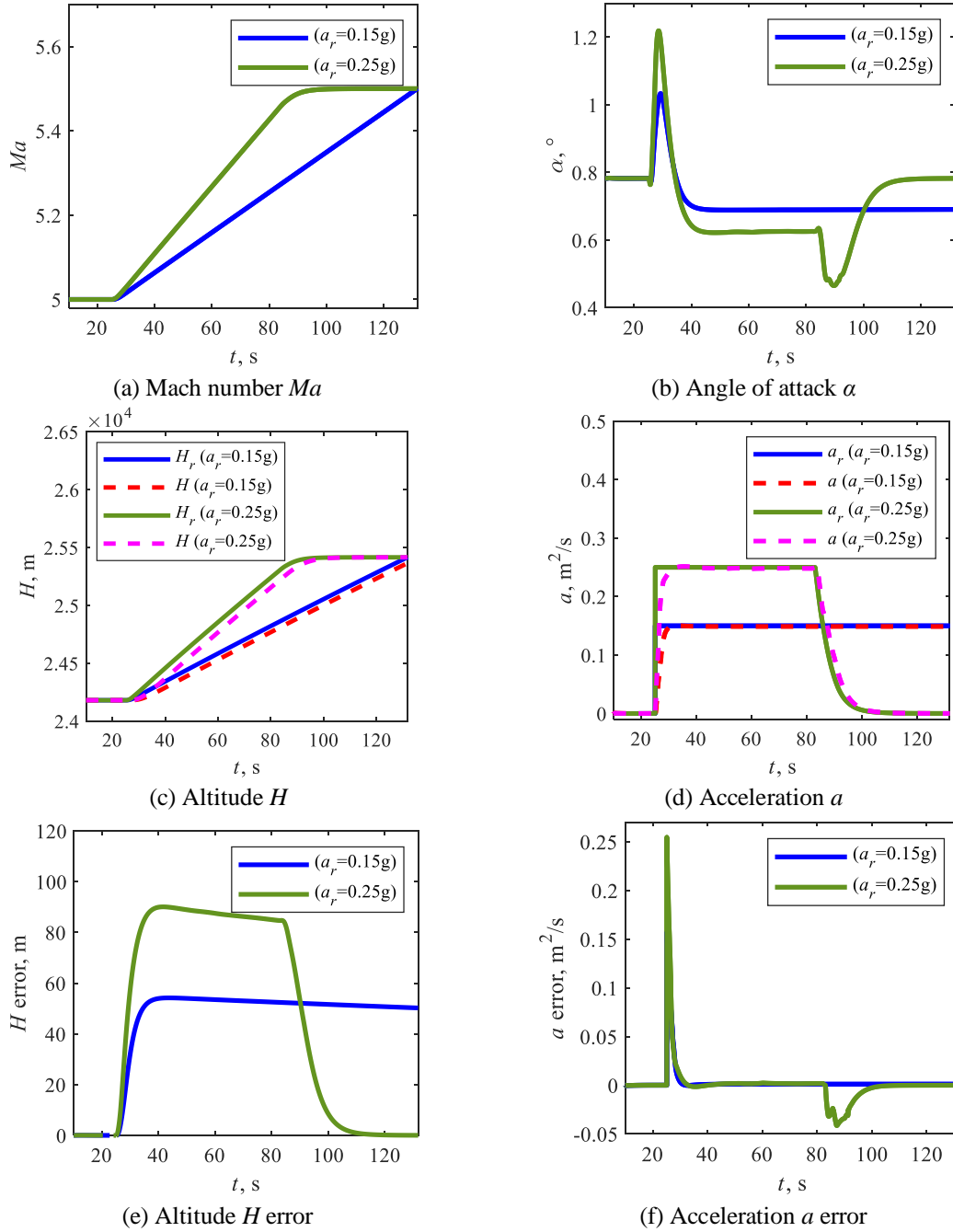


Fig. 6 Comparison of the outputs of the vehicle attitude control system between $a_r=0.15$ g and $a_r=0.25$ g

acceleration of the vehicle quickly keeps up with the command signal and maintains at the steady-state value of 0.15 g without obvious errors. In Fig. 7, the thrust and inlet steady margin of the scramjet under acceleration command 0.15 g are indicated. The tracking error of thrust and inlet

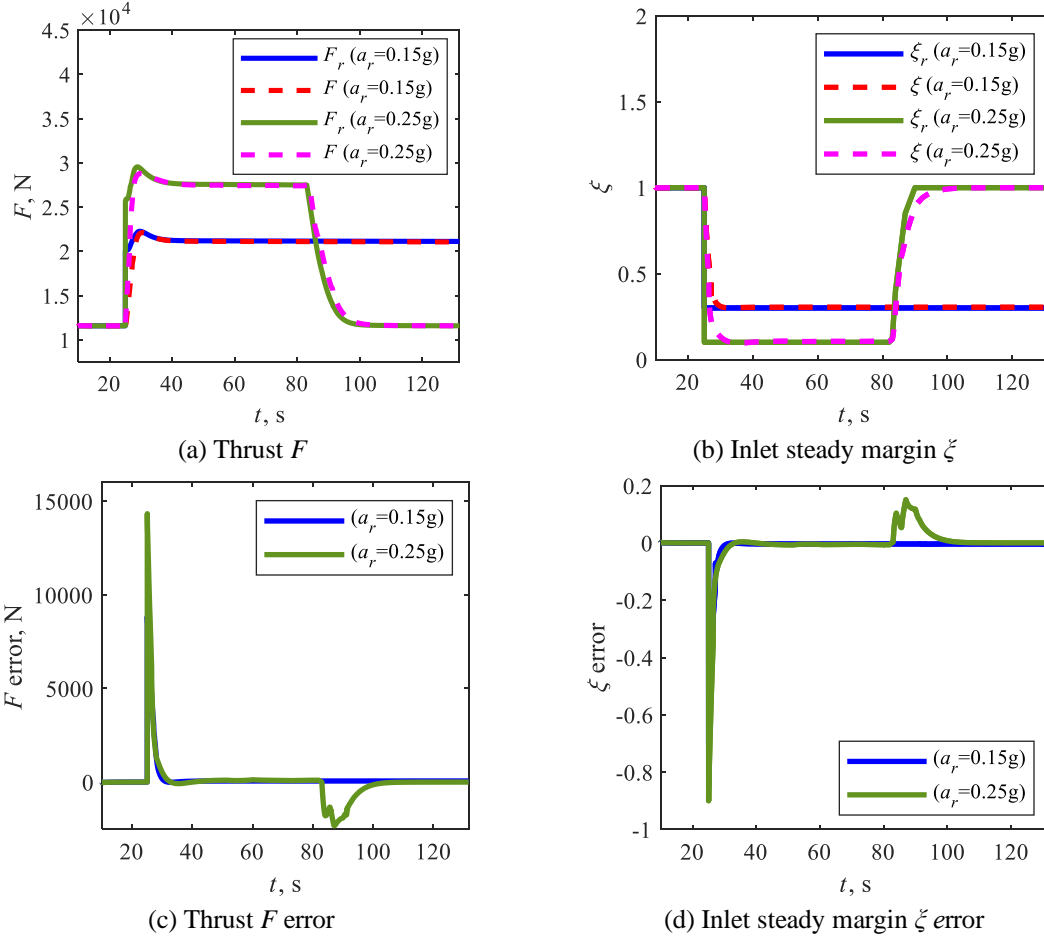


Fig. 7 Comparison of the outputs of scramjet multivariable control system between $a_r=0.15 \text{ g}$ and $a_r=0.25 \text{ g}$

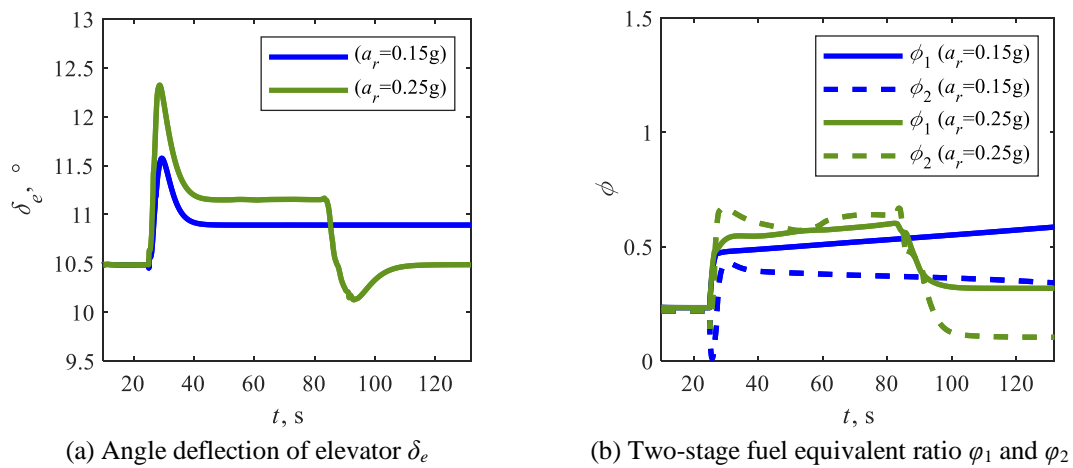


Fig. 8 Comparison of the outputs of the vehicle attitude controller and engine multivariable controller between $a_r=0.15 \text{ g}$ and $a_r=0.25 \text{ g}$

steady margin is close to zero in Fig. 7(c) and (d). Compared with the altitude tracking response of the vehicle, the engine output tracking response is faster, which is also the key to the successful design of the integrated control system. In Fig. 8, the outputs of the angle deflection of elevator and the two-stage fuel equivalent ratio are shown in blue line. The angle deflection of elevator rose first and then fell, and then stabilized at 11° in Fig. 8(a). This is because the thrust command rose and then fell. The control system changes the aerodynamic pitch moment by adjusting the angle deflection of elevator to counteract the thrust moment, which stabilizes the vehicle attitude. The two-stage fuel equivalent ratio is constantly changing according to the requirements of the control command in Fig. 8(b). Overall, the integrated control system can effectively guarantee the attitude stability of the vehicle during the acceleration process, and can ensure the safe operation of the propulsion system while maintaining the thrust performance through the engine multivariable control loop

4.2 Limiting case ($a=0.25\text{ g}$)

With the increase of acceleration command, the safety problem of the propulsion system of air-breathing hypersonic vehicle becomes more and more prominent, which is because a larger acceleration command signal will be converted into a larger thrust command signal, so that the scramjet runs closer to the safety boundary under the same operating condition. The performance of the model output is that the inlet steady margin changes with the command signal. Next, the simulation process of acceleration command signal 0.25 g is given to study the significance of propulsion system safety in the integrated control of the air-breathing hypersonic vehicle. We let the air-breathing hypersonic vehicle operate under the command of the integrated control system with an acceleration of 0.25 g , and fly from $Ma\ 5.0$ to $Ma\ 5.5$. In Fig. 6, the solid green line and the dotted pink line show the state output of the aircraft attitude control loop when the air-breathing hypersonic vehicle climbs at an acceleration of 0.25 g . With the similar acceleration command, Fig. 7 indicates the performance output of the engine multivariable control loop by solid green line and the dotted pink line, and Fig. 8 gives the controller output of both control loops by solid green line and dotted green line.

As can be seen from Fig. 6(a), increasing the acceleration command value, the acceleration process is completed around 90 seconds, which is 41 seconds faster than normal case 0.15 g . Currently, the angle of attack is about 0.63° , which is smaller than the normal case. For the output results of the vehicle altitude, the tracking error is higher than the normal case, which is gradually reduced from about 90 meters to 84 meters. The acceleration error of the vehicle is basically near 0 under the guarantee of the thrust. The acceleration of limiting case is completed successfully. However, the safe index inlet steady margin has changed during this process. The comparison results of engine thrust and inlet stability margin output with acceleration commands of 0.15 g and 0.25 g are given in Fig. 7. To obtain higher acceleration, it is necessary to provide greater thrust. Fig. 7(a) shows the thrust demand increases nearly 6400 N in limiting case than normal case. As a matter of fact, the safety of the scramjet faces challenges under limiting case. In Fig. 7(b), the command signal of the inlet steady margin must be adjusted down from 0.3 to 0.1 to meet the thrust performance requirements when the acceleration is 0.25 g . It can also be said that 0.1 is the maximum command value of the inlet steady margin in limiting case. If the inlet steady margin command is set beyond this value, the engine will not be able to satisfy the thrust requirements. The solid green line and dotted pink line in Fig. 7(b) indicate that the maximum set value of the inlet steady margin is awfully close to the safety boundary zero. Thus, a small disturbance may

cause the inlet unstart resulting in disastrous consequences. The research results show that it is inaccurate to study the control of air-breathing hypersonic vehicle in isolation from the specific working conditions of the engine. When operating near the limiting condition, the safety of the propulsion system deserves special attention from the integrated control system of the hypersonic vehicle. In Fig. 8(a), the change pattern of elevator deflection angle is consistent with thrust. Again, the control system is shown to maintain the attitude stability of the vehicle by changing the angle deflection of elevator to counteract the thrust moment. In Fig. 8(b), the increment of the second stage fuel equivalent ratio φ_2 is larger than that of the first stage φ_1 . Because the stability margin is mainly determined by φ_1 . When φ_1 makes the stability margin remain at 0.1, however, it can not meet the thrust demand. Then φ_2 is needed to supplement this part of thrust, and the gain of φ_2 to thrust is less, so the increment of φ_2 is greater than φ_1 .

5. Conclusions

This paper studies the integrated control of an air-breathing hypersonic vehicle considering the safety of propulsion system. The effectiveness and superiority of the integrated control system are verified through the comparison of normal and limiting acceleration case for an air-breathing hypersonic scramjet coupling model. The main conclusions are as follows:

- (1) We combine the longitudinal rigid body dynamics model of air-breathing hypersonic vehicles and quasi-one-dimensional dual-mode scramjet model to build a vehicle/engine coupling model with inlet steady margin. Based on the coupling model, the external loop control system converts the acceleration command to thrust command and acts on the engine multivariable controller of the internal loop control system. Combined with the inlet steady margin command, the engine multivariable controller ensures the thrust output while avoiding the inlet unstart. Meanwhile, with the thrust provided by the engine, the vehicle attitude controller maintains the stability of the vehicle by adjusting the angle deflection of elevator. The change in the angle deflection of elevator causes a change in the angle of attack, which further affects the engine output by changing the incoming flow conditions.
- (2) In normal acceleration case $a_r=0.15$ g and limiting case $a_r=0.25$ g, the results show that the integrated control system tracks the altitude and speed of the vehicle well and is able to maintain the attitude stability of the vehicle by adjusting the angle deflection of elevator to counteract the thrust moment, while allocating the two-stage fuel equivalent ratio to meet the thrust performance and safety margin of the engine. The difference is that greater acceleration means that the engine needs to provide higher thrust, which brings the propulsion system closer to extreme dangerous conditions. In limiting case $a_r=0.25$ g, the inlet steady margin needs to be reduced from 0.3 to 0.1, which is too close to inlet unstart safety margin $\zeta=0$, to provide enough engine thrust to meet the vehicle control requirements. Therefore, the integrated control considering the safety of the propulsion system is a significant way that ensure the acceleration effective and safe.

Acknowledgements

This research work is supported by the Fundamental Research Funds for the Central Universities (Grant No. FRFCU5710094620, Grant No. HIT.BRET.2021006).

References

- An, H., Wu, Q., Wang, G., Guo, Z. and Wang, C. (2020), "Simplified longitudinal control of air-breathing hypersonic vehicles with hybrid actuators", *Aerosp. Sci. Technol.*, **104**, 105936. <https://doi.org/10.1016/j.ast.2020.105936>.
- Baumann, E., Pahle, J.W., Davis, M.C. and White, J.T. (2013), "X-43A flush airdata sensing system flight-test results", *J. Spacecr. Rocket.*, **47**(1), 48-61. <https://doi.org/10.2514/1.41163>.
- Bolender, M.A. (2009), "An overview on dynamics and controls modelling of hypersonic vehicles", *2009 American Control Conference*, St. Louis, MO, June.
- Bolender, M.A. and Doman, D.B. (2005), "A non-linear model for the longitudinal dynamics of a hypersonic air-breathing vehicle", *AIAA Guidance, Navigation and Control Conference and Exhibit*, San Francisco, California, August.
- Bolender, M.A. and Doman, D.B. (2007), "Nonlinear longitudinal dynamical model of an air-breathing hypersonic vehicle", *J. Spacecr. Rocket.*, **44**, 374-387. <https://doi.org/10.2514/1.23370>.
- Burcham, Jr, F., Ray, R., Conners, T. and Walsh, K. (1998), "Propulsion flight research at NASA Dryden from 1967 to 1997", *Proceedings of the 34th AIAA/ASME/SAE/ASEE Joint Propulsion Conference and Exhibit*, Cleveland, July.
- Cheng, X., Wang, P. and Tang, G. (2019), "Fuzzy-reconstruction-based robust tracking control of an air-breathing hypersonic vehicle", *Aerosp. Sci. Technol.*, **86**, 694-703. <https://doi.org/10.1016/j.ast.2019.01.041>.
- Cui, T. (2014), "Simplified procedure for controlling pressure distribution of a scramjet combustor", *Chin. J. Aeronaut.*, **27**(5), 1137-1141. <https://doi.org/10.1016/j.cja.2014.08.015>.
- Doyle, J.C., Glover, K., Khargonekar, P.P. and Francis, B.A. (1989), "State-space solutions to standard H₂ and H_∞ control problems", *IEEE Trans. Autom. Control*, **34**, 831-847. <https://doi.org/10.1109/9.29425>.
- Echols, J.A., Puttannaiah, K., Mondal, K. and Rodriguez, A.A. (2013), "Fundamental control system design issues for scramjet-powered hypersonic vehicles", *AIAA Guidance, Navigation and Control Conference*, Kissimmee, Florida, USA.
- Fiorentini, L., Serrani, A., Bolender, M.A. and Doman, D.B. (2009), "Nonlinear robust adaptive control of flexible air-breathing hypersonic vehicles", *J. Guid. Control Dyn.*, **32**, 401-416. <https://doi.org/10.2514/1.39210>.
- Gahinet, P. and Apkarian, P. (1994), "A linear matrix inequality approach to h control", *Int. J. Robust Nonlin. Control*, **4**(4), 421-448. <https://doi.org/10.1002/rnc.4590040403>.
- Groves, K.P., Serrani, A., Yurkovich, S., Bolender, M.A. and Doman, D.B. (2006), "Anti-windup control for an air-breathing hypersonic vehicle model", *AIAA Guidance, Navigation and Control Conference and Exhibit*, Keystone, Colorado, August.
- Huo, Y., Mirmirani, M., Ioannou, P. and Kuipers, M. (2006), "Altitude and velocity tracking control for an air-breathing hypersonic cruise vehicle", *AIAA Guidance, Navigation and Control Conference and Exhibit*, Keystone, Colorado, USA.
- Lee, Y.J., Kang, S.H. and Yang, S.S. (2015), "A study on the hypersonic air-breathing engine ground test facility composition and characteristics", *J. Kor. Soc. Propul. Eng.*, **19**(6), 81-90. <https://doi.org/10.6108/KSPE.2015.19.6.081>.
- Li, J., Li, D., Wu, G. and Liu, K. (2021). Flight-Propulsion Integration Dynamic Analysis and Adaptive Control of the Hypersonic Vehicle at Wide-Range Mach Numbers. *IEEE Access*, **10**, 6954-6965. <https://doi.org/10.1109/ACCESS.2021.313661>.
- Li, N., Chang, J., Xu, K., Yu, D. and Song, Y. (2019), "Closed-loop control of shock train in inlet-isolator with incident shocks", *Exp. Therm. Fluid Sci.*, **103**, 355-363. <https://doi.org/10.1016/j.expthermflusci.2019.01.033>.
- Lv, C., Chang, J., Dong, Y., Ma, J. and Xu, C. (2020), "Modeling and coupling characteristics for an airframe-propulsion-integrated hypersonic vehicle", *Adv. Aircraft Spacecraft Sci.*, **7**(6), 553-570. <https://doi.org/10.12989/aas.2020.7.6.553>.

- Ma, J., Chang, J., Zhang, J., Bao, W. and Yu, D. (2018), "Control-oriented modeling and real-time simulation method for a dual-mode scramjet combustor", *Acta Astronaut.*, **153**, 82-94. <https://doi.org/10.1016/j.actaastro.2018.10.002>.
- Ma, J., Chang, J., Zhang, J., Bao, W. and Yu, D. (2019), "Control-oriented unsteady one-dimensional model for a hydrocarbon regeneratively-cooled scramjet engine", *Aerosp. Sci. Technol.*, **85**, 158-170. <https://doi.org/10.1016/j.ast.2018.12.012>.
- Mooij, E. (2001), "Numerical investigation of model reference adaptive control for hypersonic aircraft", *J. Guid. Control Dyn.*, **24**, 315-323. <https://doi.org/10.2514/2.4714>.
- Mu, C., Ni, Z., Sun, C. and He, H. (2017), "Air-breathing hypersonic vehicle tracking control based on adaptive dynamic programming", *IEEE Trans. Neur. Netw. Learn. Syst.*, **28**(3), 584-598. <https://doi.org/10.1109/TNNLS.2016.2516948>.
- Parker, J.T., Serrani, A., Yurkovich, S., Bolender, M.A. and Doman, D.B. (2007), "Control-oriented modeling of an air-breathing hypersonic vehicle", *J. Guid. Control Dyn.*, **30**(3), 856-869. <https://doi.org/10.2514/1.27830>.
- Rodriguez, A., Dickeson, J., Cifdaloz, O., Kelkar, A., Vogel, J., Soloway, D., McCullen, R., Benavides, J. and Sridharan, S. (2008), "Modeling and control of scramjet-powered hypersonic vehicles: Challenges, trends, and tradeoffs", *AIAA Guidance, Navigation and Control Conference and Exhibit*, Honolulu, Hawaii, August.
- Sigthorsson, D.O. (2008), "Control-oriented modeling and output feedback control of hypersonic air-breathing vehicles", Ph.D. Dissertation, The Ohio State University, Columbus, U.S.A.
- Wang, F., Guo, Y., Wang, K., Zhang, Z., Hua, C.C. and Zong, Q. (2019), "Disturbance observer based robust backstepping control design of flexible air-breathing hypersonic vehicle", *IET Control Theor. Appl.*, **13**(4), 572-583. <http://doi.org/10.1049/iet-cta.2018.5482>.
- Yao, Z.H., Bao, W., Chang, J.T., Yu, D.R. and Tang, J.F. (2010), "Modelling for couplings of an airframe-propulsion integrated hypersonic vehicle with engine safety boundaries", *Proc. Inst. Mech. Eng. Part G J. Aerosp. Eng.*, **224**(1), 43-55. <https://doi.org/10.1243/09544100JAERO618>.
- Yu, H., Guo, Y., Yan, X. and Wang, J. (2022), "Flight/propulsion integrated control of over-under TBCC engine based on GA-LQR method", *Aerosp.*, **9**(10), 621. <https://doi.org/10.3390/aerospace9100621>.
- Zhang, J., Kang, W., Li, A. and Yang, L. (2016), "Integrated flight/propulsion optimal control for DPC aircraft based on the GA-RPS algorithm", *Proc. Inst. Mech. Eng., Part G: J. Aerosp. Eng.*, **230**(1), 157-171. <https://doi.org/10.1177/0954410015588933>.
- Zheng, J., Chang, J., Ma, J. and Yu, D. (2019), "Modeling and analysis for integrated airframe/propulsion control of vehicles during mode transition of over-under Turbine-Based-Combined-Cycle engines", *Aerosp. Sci. Technol.*, **95**, 105462. <https://doi.org/10.1016/j.ast.2019.105462>.

EC

Nomenclature

a	acceleration
\bar{c}	reference length of engine
D	drag
e	error
f	nonlinear differentiable functions
g	acceleration of gravity
G	controlled plant
H	altitude

I_{yy}	moment of inertia
J	quadratic performance indicators
K	controller
K_{vv}	controller of attitude stability
K_{vH}	controller of altitude tracking
L	lift
m	vehicle mass
M	pitching moment
Ma	Mach number
P	generalized controlled plant
q	pitch rate
s	reference area
S	sensitivity function
T	sensitivity function
F	thrust
F_r	command of thrust
u	controller output signal
v	controller input signal
V	velocity
w	external input signal
W_1	performance weight function
W_2	input weight function
W_3	output weight function
x	state variable
y	output variable
z	performance output signal
zT	force-arm of the propulsion system

Greek letters

α	angle of attack
δ_e	angle deflection of elevator
φ_1	first stage fuel equivalent ratio
φ_2	second stage fuel equivalent ratio
θ	pitch angle density
ω	integral of altitude tracking error
ζ	inlet steady margin

Subscripts

p	engine
r	command signal
v	vehicle

Appendix A

The aerodynamic coefficient of polynomial fitting functions of lift L , drag D and pitching moment M in Eq. (2) is described as

$$\begin{cases} C_L(\alpha, \delta_e) = C_L^\alpha \alpha + C_L^{\delta_e} \delta_e + C_L^0 \\ C_D(\alpha, \delta_e) = C_D^{\alpha^2} \alpha^2 + C_D^\alpha \alpha + C_D^{\delta_e^2} \delta_e^2 + C_D^{\delta_e} \delta_e + C_D^0 \\ C_M(\alpha, \delta_e) = C_{M,\alpha}^{\alpha^2} \alpha^2 + C_{M,\alpha}^\alpha \alpha + C_{M,\alpha}^0 + c_e \delta_e \end{cases} \quad (\text{A1})$$

The value of the coefficient is shown in Table 3 to Table 5.

Table 3 Lift fitting coefficient

Coefficient	Value	Unit
C_L^α	4.6773×100	rad^{-1}
$C_L^{\delta_e}$	7.6224×10^{-1}	rad^{-1}
C_L^0	-1.8714×10^{-2}	—

Table 4 Drag fitting coefficient

Coefficient	Value	Unit
$C_D^{\alpha^2}$	5.8224×100	rad^{-2}
C_D^α	-4.5315×10^{-2}	rad^{-1}
$C_D^{\delta_e^2}$	8.1993×10^{-1}	rad^{-2}
$C_D^{\delta_e}$	2.7699×10^{-4}	rad^{-1}
C_D^0	1.0131×10^{-2}	—

Table 5 Pitching moment fitting coefficient

Coefficient	Value	Unit
$C_{M,\alpha}^{\alpha^2}$	6.2926×100	rad^{-2}
$C_{M,\alpha}^\alpha$	2.1335×100	rad^{-1}
$C_{M,\alpha}^0$	1.8979×10^{-1}	—
c_e	-1.2897×100	rad^{-1}